

# Heme oxygenase 1 defects lead to reduced chlorophyll in *Brassica napus*

Lixia Zhu<sup>1</sup> · Zonghui Yang<sup>2</sup> · Xinhua Zeng<sup>3</sup> · Jie Gao<sup>1</sup> · Jie Liu<sup>1</sup> · Bin Yi<sup>1</sup> ·  
Chaozhi Ma<sup>1</sup> · Jinxiong Shen<sup>1</sup> · Jinxing Tu<sup>1</sup> · Tingdong Fu<sup>1</sup> · Jing Wen<sup>1</sup>

Received: 27 May 2016 / Accepted: 9 January 2017 / Published online: 20 January 2017  
© Springer Science+Business Media Dordrecht 2017

**Abstract** We previously described a *Brassica napus* chlorophyll-deficient mutant (*ygl*) with yellow-green seedling leaves and mapped the related gene, *BnaC.YGL*, to a 0.35 cM region. However, the molecular mechanisms involved in this chlorophyll defect are still unknown. In this study, the *BnaC07.HO1* gene (equivalent to *BnaC.YGL*) was isolated by the candidate gene approach, and its function was confirmed by genetic complementation. Comparative sequencing analysis suggested that *BnaC07.HO1* was lost in the mutant, while a long noncoding-RNA was inserted into the promoter of the homologous gene *BnaA07.HO1*. This insert was widely present in *B. napus* cultivars and down-regulated *BnaA07.HO1* expression. *BnaC07.HO1* was highly expressed in the seedling leaves and encoded heme oxygenase 1, which was localized in the chloroplast. Biochemical analysis showed that *BnaC07.HO1* can catalyze heme conversion to form biliverdin IX $\alpha$ . RNA-seq analysis revealed that the loss of *BnaC07.HO1*

impaired tetrapyrrole metabolism, especially chlorophyll biosynthesis. According, the levels of chlorophyll intermediates were reduced in the *ygl* mutant. In addition, gene expression in multiple pathways was affected in *ygl*. These findings provide molecular evidences for the basis of the yellow-green leaf phenotype and further insights into the crucial role of HO1 in *B. napus*.

**Keywords** *Brassica napus* · Yellow-green leaf · Heme oxygenase 1 · LncRNA insertion · Tetrapyrrole metabolism · Chlorophyll biosynthesis

## Introduction

Tetrapyrroles play essential roles in various biological processes, including photosynthesis and respiration. In higher plants, there are four classes of tetrapyrroles: chlorophyll, heme, siroheme, and phytychromobilin (P $\Phi$ B), which are derived from a common biosynthetic pathway. Phytychromobilin differs from the other three tetrapyrroles because it is a linear tetrapyrrole, whereas the others have a closed macrocycle. Phytychromes (phys) utilize covalently bound phytychromobilin chromophores, which can mediate photoconversion between red-absorbing and far-red-absorbing forms. Phys influence seed germination, chloroplast development, leaf growth, pigmentation, circadian rhythms, flowering time and senescence (Franklin and Quail 2010; Rockwell et al. 2006).

The biosynthetic pathways for phytychromobilin and chlorophyll share precursors from 5-aminolevulinic acid (ALA) to protoporphyrin IX (Proto IX). Proto IX is located at the branch point of heme and chlorophyll biosynthesis. At this point, ferrochelatase inserts Fe<sup>2+</sup> into Proto IX to form protoheme (heme b), whereas magnesium chelatase

**Electronic supplementary material** The online version of this article (doi:10.1007/s11103-017-0583-y) contains supplementary material, which is available to authorized users.

✉ Jing Wen  
wenjing@mail.hzau.edu.cn

- <sup>1</sup> National Key Laboratory of Crop Genetic Improvement, National Sub-center of Rapeseed Improvement in Wuhan, Huazhong Agricultural University, Wuhan 430070, China
- <sup>2</sup> Shandong Key Laboratory of Greenhouse Vegetable Biology, Shandong Branch of National Vegetable Improvement Center, Institute of Vegetables and Flowers, Shandong Academy of Agricultural Sciences, Jinan 250100, China
- <sup>3</sup> Key Laboratory of Biology and Genetic Improvement of Oil Crops Oil Crops Research the Chinese Institute of Academy of Agricultural Sciences., Ministry of Agriculture, Wuhan 430062, China

inserts  $Mg^{+}$  into Proto IX to form Mg-Proto IX and ultimately generates chlorophyll. In chloroplasts, protoheme is oxidatively cleaved by heme oxygenase (HO) to form biliverdin IX $\alpha$  (BV IX $\alpha$ ), releasing  $Fe^{2+}$  and carbon monoxide (CO). The enzyme P $\Phi$ B synthase (HY2) then converts BV IX $\alpha$  to 3Z-P $\Phi$ B, which is subsequently isomerized to 3E-P $\Phi$ B and assembled into the functional holo-phys (Tanaka et al. 2011). Although the heme/P $\Phi$ B and chlorophyll biosynthetic pathways have different end products, experimental data indicate that they are coordinately regulated by modulating ALA synthesis, which is the rate-limiting step regulating the influx of metabolites into tetrapyrrole synthesis (Brzezowski et al. 2015; Czarnecki and Grimm 2012). For example, in HO1 mutants (including *Arabidopsis hy1*, tomato *yg-2*, pea *pcd1*, maize *elm2* and rice *se5*) and HY2 mutants (including *Arabidopsis hy2*, tomato *au*, pea *pcd2*, and maize *elm1*), heme/P $\Phi$ B biosynthesis was severely limited, leading to chlorophyll level reductions and leaf chlorosis, even though the chlorophyll branch was not blocked (Davis et al. 2001; Emborg et al. 2006; Izawa et al. 2000; Muramoto et al. 1999; Sawers et al. 2004; Shi et al. 2013; Terry 1997; Terry and Kendrick 1996; Weller et al. 1996, 1997).

In *Arabidopsis*, a single gene encoding P $\Phi$ B synthase and four genes encoding HO were identified. Based on their amino acid sequence similarities, these four HOs were divided into two subfamilies: HO1 (including HO1, HO3, and HO4) and HO2. HO1 subfamily members contain the canonical HO active site, while HO2 lacks a positionally conserved histidine residue in the active site that is usually involved in heme–iron coordination (Emborg et al. 2006; Gisk et al. 2010; Shekhawat and Verma 2010). Among the four *Arabidopsis HO* genes, *HO1* shows the highest expression level whereas the expression levels of *HO3* and *HO4* are extremely low. *HO2* expression is slightly induced by light at the onset of greening (Matsumoto et al. 2004). Recently, several studies have demonstrated that HO1 or its catalytic product CO is involved in all aspects of plant development and environmental adaptation, including seed development (Prasad et al. 2012), lateral root formation (Cao et al. 2011, 2007), root development (Ling et al. 2009; Xuan et al. 2008), programmed cell death (Wu et al. 2011), stomatal closure (Xie et al. 2015), salinity and osmotic stress tolerance (Cao et al. 2011; Verma et al. 2015; Xie et al. 2011), heavy metal toxicity (Han et al. 2014; Shen et al. 2011), UV radiation (Xie et al. 2012; Yannarelli et al. 2006), reactive oxygen species damage (Lee et al. 2012), and hormonal signaling (Xie et al. 2015; Zhai et al. 2007).

*Brassica napus* (AACC,  $2n=38$ ) is an allopolyploid that originated from the hybridization of *Brassica oleracea* (CC,  $2n=18$ ) with *Brassica rapa* (AA,  $2n=20$ ). The A and C genomes of *B. napus* have the triplicated mesoploid structure of synteny with *Arabidopsis thaliana* (Chalhoub

et al. 2014; Parkin et al. 2002). One *Arabidopsis* locus appears to correspond to six collinear segments from the *B. napus* genome (Lysak et al. 2005; Parkin et al. 2005). Hence, it is challenging to analyze the function of a gene with multiple copies in *B. napus*. In recent years, only a few studies have investigated the interactions of *HO1* with environmental stressors in *B. napus*. Cao (2011) isolated an *HO1* cDNA through a homologous alignment analysis with *AtHO1* sequences. They proposed that *BnHO1*, which has HO catalytic properties, is a component of the signal transduction pathway in lateral root formation that responds to salinity and osmotic stress. Shen (2011) identified a full-length *BnHO1* and confirmed that overexpression of *BnHO1* can confer tolerance to Hg stress. To the best of our knowledge, *HO1* mutants have not been characterized in *B. napus*, and the role of HO1 in *B. napus* tetrapyrrole metabolism is still poorly understood.

Currently, four chlorophyll-deficient mutants have been reported in *B. napus*, but the causative molecular mechanisms remain obscure (Chu et al. 2015; Zhao et al. 2014; Zhao et al. 2000; Zhu et al. 2014). In our previous study, we obtained a *B. napus* EMS (ethyl methanesulfonate)-induced mutant (*ysl*) that exhibited reduced chlorophyll content and yellow-green leaves. The yellow-green leaf phenotype is controlled by a recessive nuclear gene, *BnaC.ygl*. *BnaC.YGL* was mapped to a 0.35 cM region that may be located in the centromeric or pericentromeric region of the N17 linkage group (Zhu et al. 2014). Thanks to the release of the *B. napus* genome (Chalhoub et al. 2014) and the mapping of *BnaC.YGL*, we successfully identified the *BnaC.YGL* gene by the candidate gene approach in this study. Further analysis indicated that the loss of *BnaC07.HO1* (equivalent to *BnaC.YGL*) in the *ysl* mutant resulted in chlorophyll deficiency in the seedling leaves and impaired tetrapyrrole metabolism, especially chlorophyll synthesis. *BnaA07.HO1*, a homolog of *BnaC07.HO1*, was also analyzed. These results provided further insights into the crucial role of HO1 in the early development of *B. napus*.

## Materials and methods

### Plant material

In this study, the chlorophyll-deficient mutant (*ysl*) with yellow-green leaves and the inbred line T6 from which the mutant was obtained were used as main plant materials. A total of 421 rapeseed inbred lines that originated from a diversity panel (Supplemental Table S7; Xu et al. 2016) were used to detect the long noncoding RNA (lncRNA) insertion in the *BnaA07.HO1* promoter. Four rapeseed inbred lines (Darmor, 4942C-5, T6, and ZS11) were used for *BnaC07.HO1* and *BnaA07.HO1* expression analysis.

The plants used in this study were grown in soil under natural conditions.

### Plant transformation

A 4.6-kb genomic DNA fragment containing the 1570-bp sequence upstream of the initiation codon, the 1416-bp *BnaC07.HO1* open reading frame, and 1551-bp of the 3' UTR was amplified from T6 using the primers H1F and H1R (Supplemental Table S6) and cloned into the *KpnI*-*SacI* sites of pCAMBIA2300 to construct the p*BnaC07.HO1*:*BnaC07.HO1* plasmid. The plasmid was introduced into *Agrobacterium tumefaciens* strain GV 3101 (pMP90) and transformed into the *ygl* mutant as previously described by Dun et al. (2011).

A 282-bp fragment of *BnaC07.HO1* cDNA was amplified using primers RHO1F and RHO1R (Supplemental Table S6), and cloned in both orientations using *PstI/XbaI* or *ScaI/KpnI* restriction sites in pCAMBIA2300. The fragments were separated by the tapetum-specific *O*-methyltransferase intron of *A. thaliana* to form a hairpin structure. The resulting RNAi construct was verified by extensive restriction digestion and DNA sequencing analysis. This plasmid was transformed into wild-type plants (T6).

### Chlorophyll and chlorophyll precursor determination

Leaf samples of wild-type (T6), chlorophyll-deficient mutant (*ygl*), and transgenic plants were harvested at the four-leaf seedling stage. Total chlorophyll (Chl) content was determined with a UVmini-1240 (Shimadzu Corporation, Kyoto, Japan) according to the methods of Arnon (1949). The ALA content was determined following the methods of Cenkci et al. (2010). The precursors, including Proto IX, Mg-Proto IX, and protochlorophyllide (Pchlde), were assayed as described by Santiago-Ong et al. (2001) and Wu et al. (2007) with minor modifications. Leaves (0.5 g fresh weight) of T6 and *ygl* were cut and homogenized in 10 mL of 90% acetone and centrifuged at 3,000 × g for 10 min. Each supernatant was washed three times with an equal volume of hexane prior to spectrophotometric analysis. Chl precursors in the acetone phase were quantified with a Shimadzu RF-5301PC fluorescence spectrophotometer using Ex400:Em632 for Proto IX, Ex440:Em633 for Pchlde, and Ex420:Em595 for Mg-Proto IX.

### RNA extraction, RT-PCR, and qRT-PCR

Total RNA samples were isolated from various tissues of *B. napus* using TRIzol reagent (Invitrogen, USA) according to the manufacturer's instructions. A sample of RNA (approximately 2 µg) was converted into cDNA with GoScript™ Reverse Transcriptase as described in the manufacturer's

instructions (Promega, USA). *BnaC07.HO1* expression was subsequently visualized by PCR using primers RT-F and RT-R (Supplemental Table S6). Real-time quantitative reverse transcription PCR (qRT-PCR) was performed with the Bio-Rad CFX96 Real-time system (Bio-Rad) and the GoTaq qPCR Master Mix (Promega, USA). The *BnaActin* gene (GenBank: AF111812.1) was used as the control gene, and relative quantification of the PCR product was performed using the comparative cycle threshold method (Supplemental Table S6). The data are expressed as the mean ± SD (n = 3 biological replicates).

### GUS assay

A 1570-bp upstream region of the *BnaC07.HO1* gene was amplified from T6 with primers Pro-F and Pro-R (Supplemental Table S6) and cloned into the binary vector pBI101. The Pro<sub>*BnaC07.HO1*</sub>:GUS construct was then introduced into *Arabidopsis* wild-type plants with the floral-dip transformation method following Jefferson et al. (1987). GUS activity was visualized by staining different stages of the heterozygous transgenic lines overnight in X-Gluc solution at 37 °C (Willemsen et al. 1998), and then tissues were cleared in 75% (v/v) ethanol.

### Subcellular localization of *BnaC07.HO1*

The full-length coding sequence of *BnaC07.HO1*, without the termination codon, was amplified using primers SL-F and SL-R (Supplemental Table S6), and inserted into the pM999GFP vector to generate a C-terminal GFP fusion product. The fusion construct was introduced into *Arabidopsis* protoplasts that were prepared from whole seedlings by polyethylene glycol (PEG)/calcium-mediated transformation (Yoo et al. 2007). The spontaneous fluorescence of Chl was used as an indicator of the chloroplast. Fluorescence signals were examined with a confocal laser microscope (Nikon).

### Expression and purification of recombinant His-tagged *BnaC07.HO1*

A synthetic gene encoding the mature (without the predicted transit peptide sequence) *BnaC07.HO1* was amplified using primers mHO1F and mHO1R (Supplemental Table S6) and inserted into a pET-28a (+) vector. The constructed vector was transferred into *Escherichia coli* strain Rosetta (DE3) pLysS. The His-tagged *BnaC07.HO1* protein was induced by 1 mM isopropyl β-D-1-thiogalactopyranoside (IPTG) at 28 °C for 3 h according to the manufacturer's instructions (Novagen), and purified through a Ni-NTA column and Sephadex® G-25 chromatography (Cao et al. 2011). The pooled protein solutions

were dialyzed against a reaction buffer (100 mM HEPES-NaOH buffer, pH 7.2) and then used for subsequent biochemical experiments.

### Western blotting

The purified fusion protein was detected by western blotting following the methods of Jing et al. (2012) and Zhao et al. (2015). Homogenates obtained for HO activity assays were analyzed. Fifty micrograms of protein from homogenates was separated by 12% SDS-PAGE and transferred onto a membrane (PVDF type, Millipore). Non-specific binding of antibodies was blocked with 2% bovine serum albumin in phosphate-buffered saline (PBS, pH 7.4) for 2 h at 4 °C. Membranes were then incubated with a mouse primary antibody against His (Thermo Fisher Scientific), diluted 1:2,000 in PBS buffer for 2 h at room temperature. Immune complexes were detected using horseradish peroxidase-conjugated goat anti-mouse IgG (Thermo Fisher Scientific).

### Enzymatic activity assay

HO activity was assayed as previously described with minor modifications (Muramoto et al. 2002; Xu et al. 2012). Changes in absorbance between 350 and 750 nm were monitored for 20 min at 25 °C. The concentration of BV IX $\alpha$  was estimated using an extinction coefficient at 680 nm of 6.25 mM<sup>-1</sup> cm<sup>-1</sup> in 100 mM HEPES-NaOH buffer (pH 7.2). Reaction rates for the formation of BV IX $\alpha$  were determined by measuring absorbance at 680 nm for 10 min. Values for the maximum reaction rate ( $V_{\max}$ ) and the Michaelis–Menten constant ( $K_m$ ) were calculated using a Lineweaver–Burk plot. Temperature dependence of the HO reaction was measured between 10 and 45 °C. The pH dependence of the reaction was monitored between pH 6.5 and 8.0 in 100 mM HEPES-NaOH buffer, and the standard assay conditions were used as described above.

### RNA sequencing

Total RNA samples were extracted from the leaves of the *ygl* mutant and the transgenic line TP10. The transcriptomes were sequenced on an Illumina HiSeqTM 2000 platform (Illumina, USA). Gene expression levels were calculated using the reads per kilobase per million (RPKM) method (Mortazavi et al. 2008). To screen for differentially expressed genes (DEGs), a *P* value corresponding to a DEG test based on the method introduced by Audic and Claverie (1997) was used. False-positive (type I errors) and false-negative (type II) errors were corrected using the false-discovery rate (FDR) method (Audic and Claverie 1997). Finally, an FDR  $\leq 0.001$  and an absolute value

of log<sub>2</sub> ratio  $\geq 1$  were set as the thresholds to determine the significance of differences in gene expression.

## Results

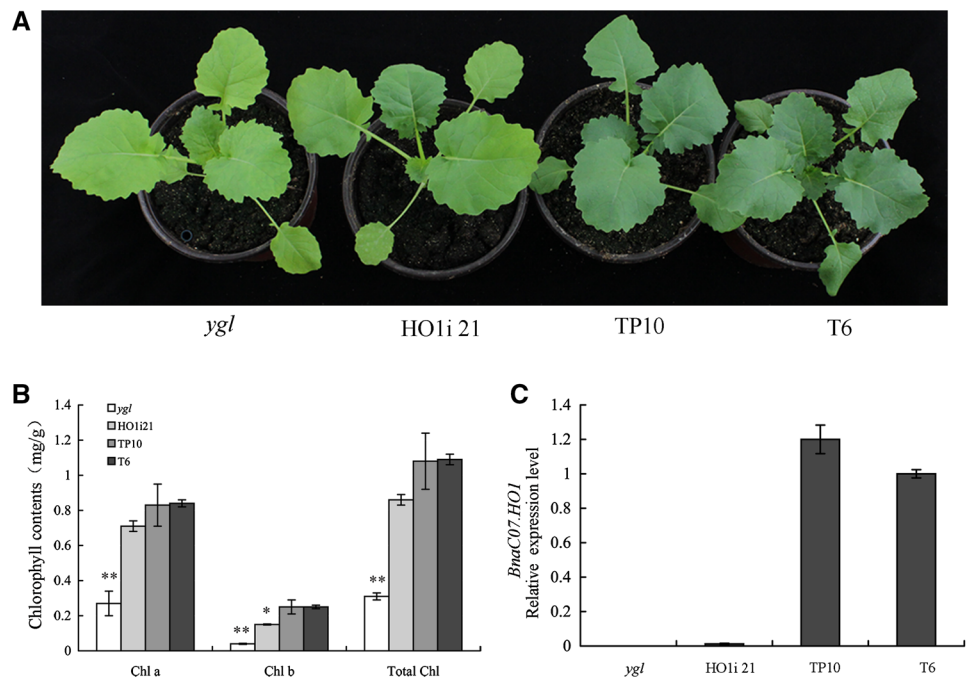
### Map-based cloning of *BnaC.YGL*

In our previous study, *BnaC.YGL* was mapped in two populations to a 0.35 cM region of linkage group N17 (C07) and 18 markers that cosegregated with this gene were developed (Zhu et al. 2014). Sequences of the closest flanking markers (BnY5 and CB10534) were submitted to BLAST searches against the *B. napus* reference genome database. The 0.35 cM region corresponded to a physical region of approximately 5,165-kb in the linkage group N17, indicating a recombination rate of 14,757-kb per cM in *B. napus*.

According to the *B. napus* annotation database, there are more than 438 predicted genes in this 5,165-kb region. An annotation analysis of these genes indicated that *BnaC07g16850D*, a syntenic ortholog of the *Arabidopsis HO1* gene that encodes an HO protein and catalyzes heme breakdown to BV IX $\alpha$  in phytochrome chromophore biosynthesis, was a promising candidate gene associated with the yellow-green leaf phenotype. In many plants, such as *Arabidopsis*, rice, tomato, pea and maize, HO1 mutants also have a yellow-green leaf phenotype during the growth period (Andres et al. 2009; Izawa et al. 2000; Muramoto et al. 1999). *BnaC07g16850D* was therefore the most likely candidate gene and was named *BnaC07.HO1*. Comparative sequencing from T6 and *ygl* showed that *BnaC07.HO1* was completely deleted in the *ygl* mutant, suggesting that it was responsible for the yellow-green leaf phenotype.

To verify this prediction, we generated a construct by inserting a 4.6-kb genomic fragment (containing the 1570-bp sequence upstream of the initiation codon, the 1416-bp *BnaC07.HO1* genomic fragment, and 1551 bp of the 3' UTR) from T6 into the vector pCAMBIA2300. We introduced this construct into *ygl* plants through *Agrobacterium*-mediated transformation. Twenty-two transgenic plants displayed the expected wild-type phenotype with green seedling leaves (Fig. 1A), suggesting that the Chl content and the proper ratio of Chl a to Chl b were recovered (Fig. 1B). We examined the T<sub>2</sub> progeny plants from six T<sub>1</sub> transgenic lines in the field, and obtained three transgenic lines with a single-copy transgene, which showed the expected Mendelian inheritance ratio of 3:1 in T<sub>2</sub> progeny (green: yellow plants,  $\chi^2 < \chi^2_{0.05} = 3.84$ ;  $P > 0.05$ ; Supplemental Table S1). The T<sub>2</sub> progeny plants displayed perfect cosegregation between the transgene and the phenotype. In addition, an RNA interference (RNAi) construct for *BnaC07.HO1* was transformed into T6 plants. The total Chl content in the T<sub>1</sub>-positive plant was intermediate between

**Fig. 1** Functional identification of *BnaC07.HO1*. **a** The phenotypic characterization of the *ysl* mutant, RNAi-transformed line HO1i21, p*BnaC07.HO1*:*BnaC07.HO1*-transformed line TP10, and T6 (wild-type phenotype). **b** The chlorophyll contents from the above four lines at the four-leaf stage. **c** The expression of *BnaC07.HO1* in the above four lines. Asterisks indicate significant differences between *ysl*, HO1i21, TP10, and T6 at the given times (*t*-test,  $n=4$ , \* $P<0.05$ , \*\* $P<0.01$ ). Error bars indicate SDs



the mutant and T6 (Fig. 1B), consistent with the expression levels of *BnaC07.HO1* in the three lines (Fig. 1C). Genetic analysis of the T<sub>2</sub> progeny plants from three positive plants was also performed (Supplemental Table S1). The yellow-green leaf phenotype of T<sub>2</sub> families cosegregated with the introduced DNA, confirming that the loss of *BnaC07.HO1* was responsible for the Chl defect in the *ysl* mutant.

### Features of *BnaC07.HO1*

The CDS sequence of *BnaC07.HO1* (846 bp) is composed of three exons and encodes a protein containing 281 amino acids including a 54-amino acid transit peptide identified with the ChloroP algorithm (<http://www.cbs.dtu.dk/services/ChloroP/>) (Fig. 2a, b). BLAST searches were performed with the *BnaC07.HO1* sequence from T6 to identify the relative homologs in the public databases. Seven homologs were identified in five species of *Brassicaceae*, including *Bra012054* in *B. rapa*, *Bol027145* in *B. oleracea*, three homologs (*BnaA07g12810D*, *BnaC07g16850D* and *GU390397.1*) in *B. napus*, *JN202587.1* in *Brassica juncea*, and *AT2g26670* in *A. thaliana*. Sequence comparisons indicated that *BnaC07.HO1* had 85% similarity to *Arabidopsis HO1*, and more than 95% similarity to other homologs (Fig. 2b). The HO signature sequence AFICH-FYNT (amino acid residues 128–136) was conserved in *BnaC07.HO1* (Shekhawat and Verma 2010). Residue H84 in *BnaC07.HO1*, which corresponds to residue H25 in animals, was maintained in these five species. Previous studies have shown that this His residue was the axial heme iron ligand, which is important for the enzymatic activity of

*HO1* (Ito-Maki et al. 1995; Sun et al. 1994). These results indicated that *Brassica HO1* might be conserved and function in heme cleavage.

To investigate the subcellular localization of *BnaC07.HO1*, we constructed a protein fusion of *BnaC07.HO1* with green fluorescent protein (GFP), which was driven by the *Cauliflower mosaic virus 35 S* promoter. This fusion construct was transformed into *Arabidopsis* protoplasts. As expected, the *BnaC07.HO1*-GFP fusion protein was localized in the chloroplasts of the protoplast (Fig. 2c–e), consistent with the subcellular localizations of *Arabidopsis* HY1, soybean *HO1* and rice *SE5* (Dixit et al. 2014; Gisk et al. 2010; Xu et al. 2012).

### Expression pattern of *BnaC07.HO1*

The transcription levels of *BnaC07.HO1* in T6 were analyzed in the seeds, roots, stems, seedling leaves, stem leaves, buds, flowers and siliques using RT-PCR and qPCR. RT-PCR analysis of total RNA extracted from T6 indicated that *BnaC07.HO1* was expressed at high levels in the seedling leaves and stem leaves. It was expressed at low levels in the buds, flowers, and siliques, but rarely in the roots, seeds, and stems (Fig. 3a). qPCR analysis verified this expression pattern (Fig. 3b). These results indicated that the *BnaC07.HO1* gene is expressed in multiple organs, consistent with the records of *AtHO1*, *BraHO1*, and *BnHO1* (Cao et al. 2011; Davis et al. 2001; Jin et al. 2012). The GUS assay also showed that rosette leaves had high expression levels of *BnaC07.HO1*. Moderate expression levels were detected in the stem leaves, buds, flowers,

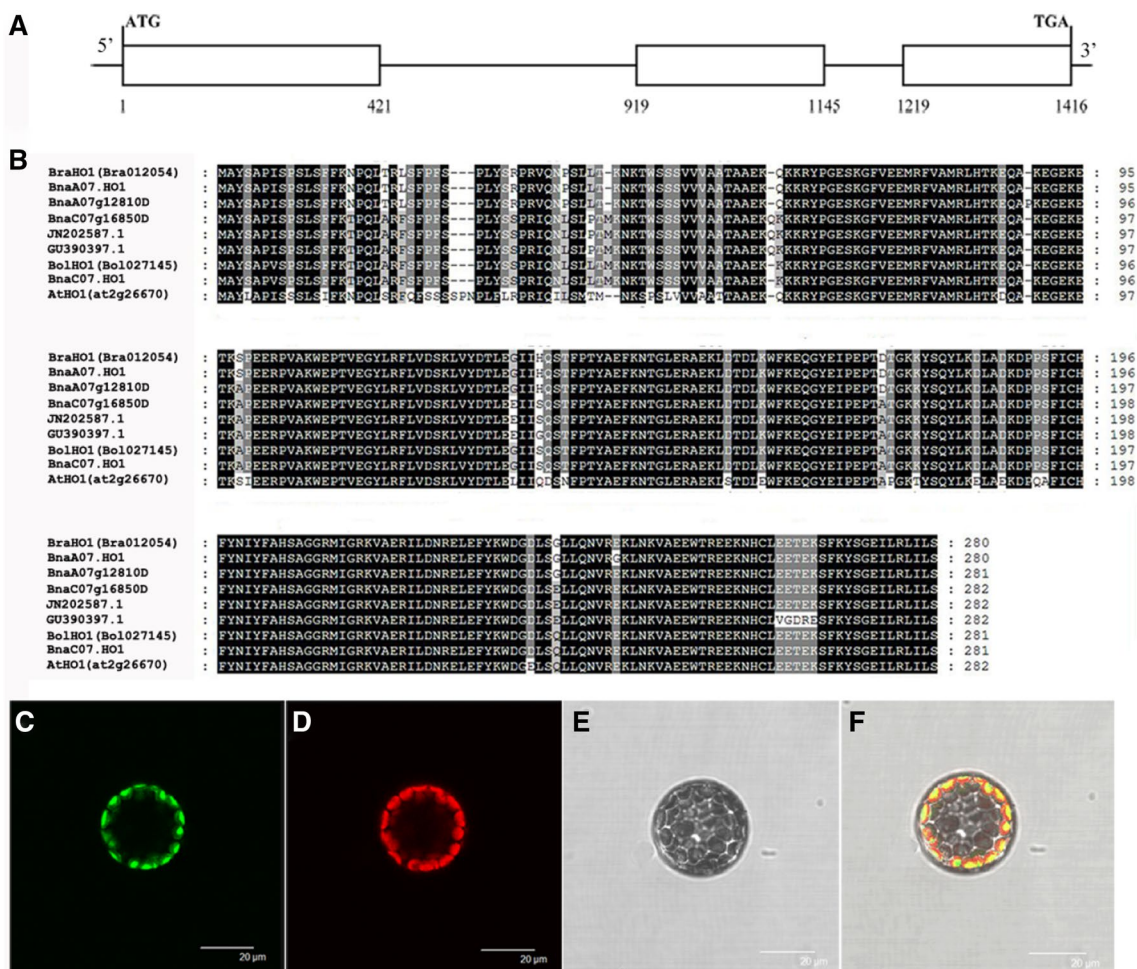


**Fig. 2** Sequence analysis and subcellular localization of the *BnaC07.HO1* gene **a** The structure of *BnaC07.HO1*. White boxes indicate exons of *BnaC07.HO1*. **b** Comparison of the amino acid sequences of HO1 in *Brassicaceae*. Sequence identifications are as follows: *B. rapa* *BraHO1* (*Bra012054*), *B. oleracea* *BolHO1* (*Bra027145*), *Brassica napus* (from Darmor) *BnaA07g12810D* and *BnaC07g16850D*, *B. napus* (from T6) *BnaA07.HO1* and *BnaC07.HO1*, *B. napus* *GU390397.1*, *B. juncea* *JN202587.1*, *A. thaliana* *AtHO1* (*at2g26670*). **c** The protoplast showed a green fluorescent signal after transformation with the *BnaC07.HO1*-GFP fusion construct. **d** The chlorophyll autofluorescence signal in the same protoplast as (c). **e** The same protoplast as (c) under bright field. **f** Merged images from (c), (d) and (e). Bars = 20 μm in (c–f).

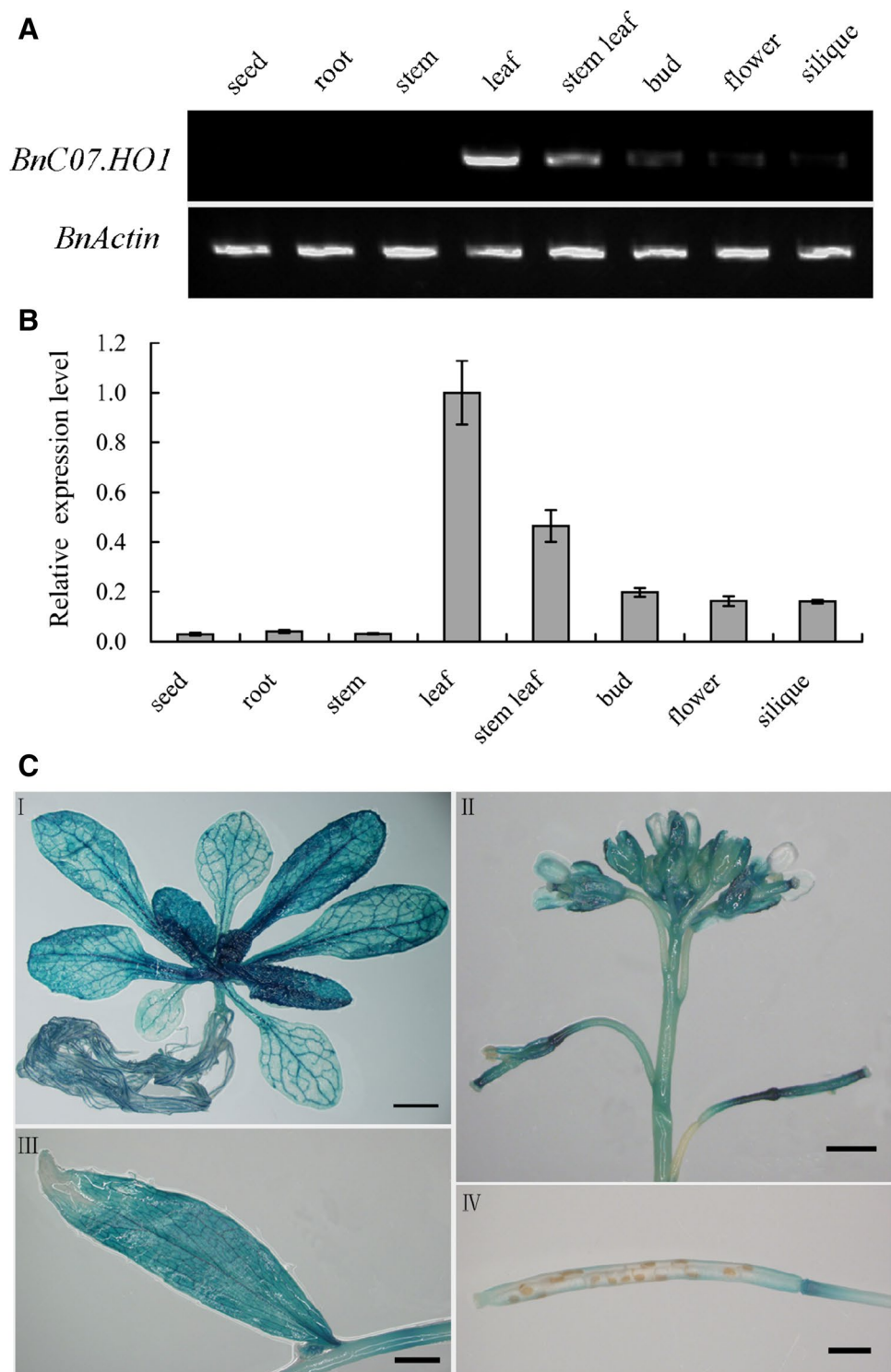
and siliques, while low levels were detected in the roots and stems (Fig. 3c). Therefore, the *BnaC07.HO1* gene is essential for the development of *B. napus*.

### Biochemical analysis of the recombinant protein

To confirm that *BnaC07.HO1* encodes an HO protein and to characterize its catalytic properties, the recombinant His-tagged protein His-*BnaC07.HO1* was expressed in *E. coli* after IPTG induction and purified by Ni-affinity chromatography. The fusion protein was approximately 30.6 kDa (including the 26.5 kDa His-*BnaC07.HO1* protein, the 0.8 kDa 6×His-tag, and the 3.3 kDa translated vector sequence) and was detected with an anti-His antibody (Fig. 4a).

The HO activity of His-*BnaC07.HO1* was measured with a spectrophotometer to detect the conversion of heme to BV IX $\alpha$ . The time-dependent absorbance was monitored between 350 and 750 nm during the reaction (Fig. 4b). The spectrum displayed a strong Soret band at 405 nm, indicating enzyme-bound heme, and a broad peak around 680 nm, indicating BV IX $\alpha$  formation. These results were similar to previous reports on heme-HO complexes and BV IX $\alpha$  (Gisk et al. 2010; Muramoto et al. 2002). The absorbance at 405 nm (bound heme) decreased over time while the absorbance at 680 nm (BV IX $\alpha$ ) increased (Fig. 4b). Kinetic parameters for purified His-*BnaC07.HO1* were determined from a Lineweaver–Burk plot (Fig. 4c). The  $V_{\max}$  was estimated as 108.8 nmol BV·h $^{-1}$  nmol $^{-1}$  protein with an apparent

**Fig. 3** Expression pattern of *BnaC07.HO1*. **a** RT-PCR expression analysis (30 cycles) of *BnaC07.HO1* in selected tissues. *BnaActin* expression was used as an internal control. **b** qPCR analysis of *BnaC07.HO1* expression in selected tissues. The expression levels were normalized to *BnaActin*. The values are presented as the mean  $\pm$  SD ( $n=3$ ). **c** GUS expression in: (I) seedling leaves and roots, (II) stems, buds and flowers, (III) stems and stem leaves and (IV) seeds and siliques of the *pBnaC07.HO1*-GUS transgenic lines in *A. thaliana*



$K_m$  value for hemin of 3.99  $\mu\text{M}$ . Moreover, the reaction rate peaked at pH 7.2 and sharply declined at lower and higher pH values (Fig. 4d). In contrast, the relative enzyme activity of His-BnaC07.HO1 increased between 10 and 40  $^{\circ}\text{C}$  (Fig. 4e), in agreement with results from

*Arabidopsis* HY1 and rice SE5 (Gisk et al. 2010; Muramoto et al. 2002; Xu et al. 2012). These results confirmed that BnaC07.HO1 acts as a catalyst in cleaving proheme to form BV IX $\alpha$ .

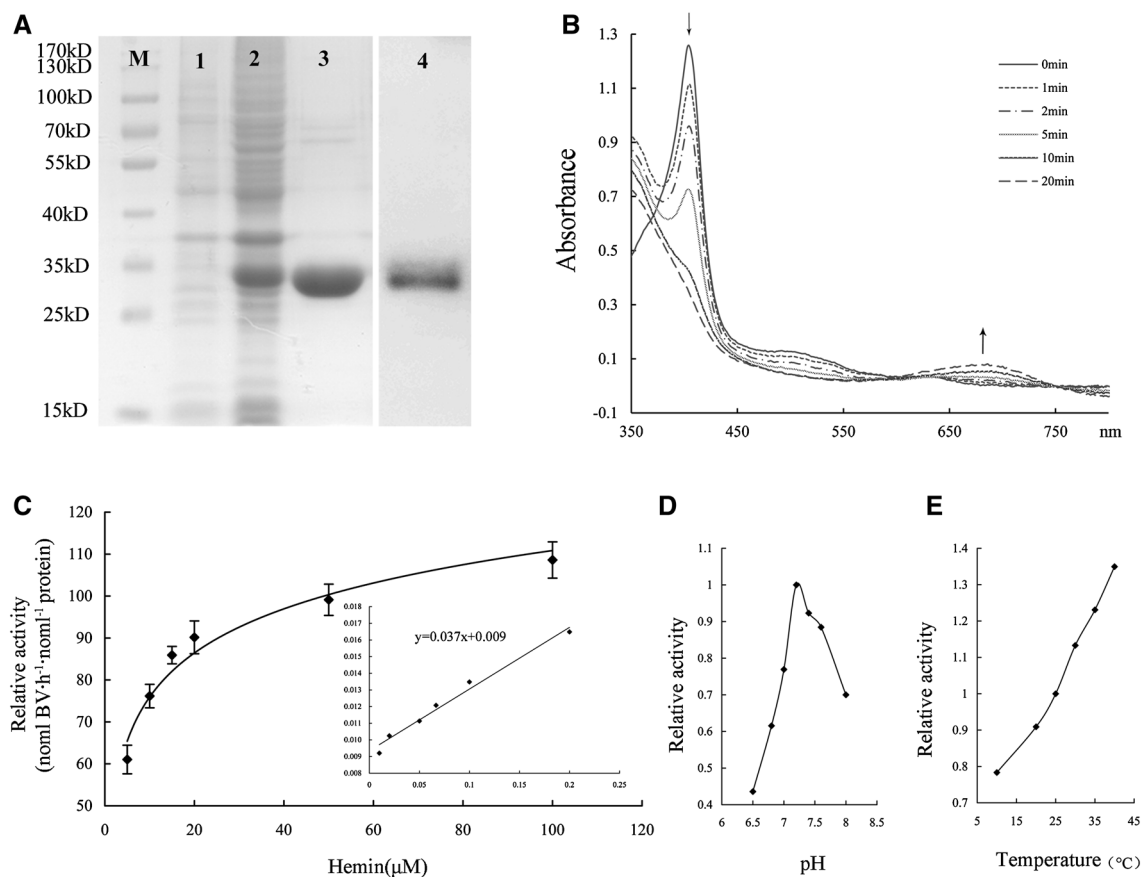


**Fig. 4** Expression and biochemical characterization of purified recombinant His-tagged mature BnaC07.HO1 (His-BnaC07.HO1) protein in *E. coli*. **a** SDS-PAGE gel of expressed protein after purification by Ni-affinity chromatography, 30  $\mu\text{g}$  protein/well. *lane M*, marker proteins; *lane 1*, control (no IPTG induction); *lane 2*, induced protein; *lane 3*, purified protein; *lane 4*, western blotting analysis of purified protein developed with anti-His. **b** Absorbance changes over time were monitored during the His-BnaC07.HO1 reaction with spectra taken at 0, 1, 2, 5, 10 and 20 min after the addition of NADPH.

Arrows indicate the directions of spectral changes during incubation. **c** Michaelis–Menten plot of the His-BnaC07.HO1 reaction for hemin concentrations of 2, 5, 10, 15, 20, and 50  $\mu\text{M}$ . The relative activity of His-BnaC07.HO1 was calculated from BV formation. Inset: Lineweaver–Burk plot of the same data. Data shown are as mean  $\pm$  SD from three independent measurements. **d** The pH dependence of the His-BnaC07.HO1 reaction. **e** The temperature dependence of the His-BnaC07.HO1 reaction.

### Loss of *BnaC07.HO1* affects the expression of the genes involved in Chl biosynthesis and photosynthesis

To better understand the mechanism underlying the regulation of *BnaC07.HO1* in seedling leaves, we compared differentially expressed genes (DEGs) in seedling leaves of the *ygl* mutant and the transgenic line TP10. In the mutant, 1296 genes were up-regulated and 562 genes were down-regulated. Ten of these DEGs were randomly selected for qPCR assays to evaluate the quality of the RNA sequencing and bioinformatics analysis (Supplemental Fig. S1 and Supplemental Table S2). According to the Kyoto Encyclopedia of Genes and Genomes (KEGG) pathway enrichment analysis for RNA-seq data, 13 DEGs were involved in tetrapyrrole metabolism, corresponding to seven enzymes in *Arabidopsis* (Supplemental Table S3). Moreover, in the

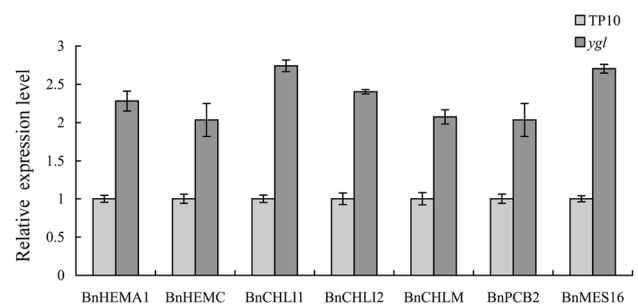


**Fig. 5** Expression levels of tetrapyrrole metabolism genes in the *ygl* mutant and the transgenic line TP10. Data are shown as the means of three biological replicates and *error bars* indicate SDs

*ysl* mutant, these genes were up-regulated, as confirmed by the qPCR assay (Fig. 5). According to the function annotations in *Arabidopsis*, four of these genes (related to HEMA1 and HEMA2) are involved in the common steps of tetrapyrrole biosynthesis, whereas eight genes (related to CHL11, CHL12, CHLM, and PCB2) are involved in the Chl biosynthesis, and one gene (related to MES16) is involved in Chl breakdown.

These up-regulated genes were tightly associated with Chl biosynthesis, so we examined the accumulation of the intermediates in Chl biosynthesis. The levels of ALA and the relative fluorescence of Proto IX, Mg-proto IX and Pchlride were analyzed in the mutant *ysl* and the transgenic line TP10. As shown in Fig. 6, the *ysl* mutant had significantly decreased levels of ALA, Proto IX, Mg-proto IX, and Pchlride, compared to the TP10 line. These data demonstrated that the loss of *BnaC07.HO1* resulted in the reduction of Chl intermediates and led to the up-regulated expressions of the genes in Chl biosynthesis.

KEGG pathway enrichment analysis showed that 26 DEGs genes associated with photosynthesis were all up-regulated, which fit well with the qPCR assay (Fig. 7). These DEGs were related to 14 genes (*PSB27*, *PSB28*, *PSBY*, *PPL1*, *PQL1*, *PQL2*, *FD1*, *FD2*, *PETE1*, *PETE2*,

*ATPD*, *LHCA5*, *LHCA6*, and *LHCB4.3*) in *Arabidopsis* (Supplemental Table S3). According to the function annotations, *PSB27*, *PSB28*, *PPL1* and *LHCB4.3* were involved in the assembly and stability of the photosystem II (PSII) supercomplex, whereas *PSB27* and *PPL1* had additional features and functioned in the repair cycle of photodamaged PSII (Nixon et al. 2010). *PQL1*, *PQL2*, *LHCA5* and *LHCA6* were required for the supercomplex formation of the chloroplast NADH dehydrogenase-like complex and photosystem I (NDH-PSI) (Peng and Shikanai 2011). *FD1*, *FD2*, *PETE1*, *PETE2* and *ATPD* were associated with the photosynthetic electron transport chain (Dal Bosco et al. 2004; Hanke and Hase 2008; Pesaresi et al. 2009). Twenty-one other pathways were affected in the *ysl* seeding leaves, including sulfur metabolism, nitrogen metabolism, carbon metabolism, carotenoid biosynthesis, and some amino acid metabolism (Supplemental Fig. S4).

### lncRNA insertion in *BnaA07.HO1* promoter down-regulates the gene expression

As a tetraploid species, *B. napus* contains two homologous copies of the *HO1* gene, namely *BnaA07.HO1* and *BnaC07.HO1*, which are located on chromosomes A07

**Fig. 6** Levels for the tetrapyrrole intermediates in the *ysl* mutant and the transgenic line TP10. **a** levels of ALA. **b** Relative fluorescence of Proto IX, Mg-proto IX, and Pchlride. Asterisks indicate significant differences at the given times (*t*-test, *n*=3, \**P*<0.05, \*\**P*<0.01). Error bars indicate SDs

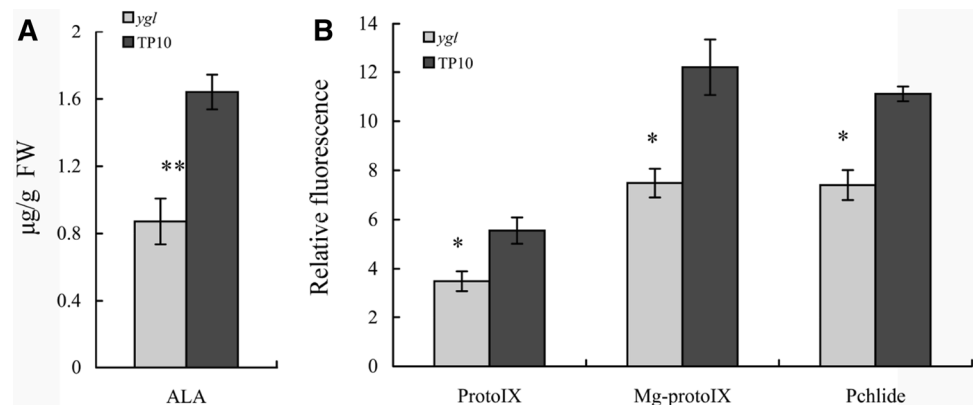
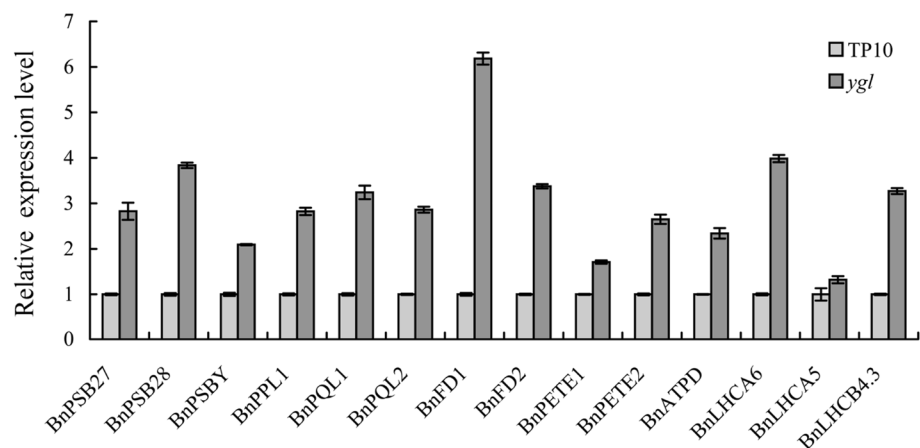


**Fig. 7** Expression levels of the genes involved in photosynthesis in the *ysl* mutant and the transgenic line TP10. Data are shown as the means of three biological replicates and error bars indicate SDs



and C07, respectively. Based on the Darmor-*bzh* reference genome (Chalhoub et al. 2014), we designed specific primers (HOF, HOR, APF, APR, CPF, and CPR in Supplemental Table S6) to identify the two homologous copies and their promoter sequences (1.6-kb sequence upstream of the initiation codon) from T6. Sequence analysis indicated that the two copies have highly homologous coding DNA sequences, but their promoter sequences had major differences in nucleotides and length (Supplemental Fig. S2). Compared with the Darmor-*bzh* reference genome, we found that a 2246-bp fragment was inserted into the *BnaA07.HO1* promoter 90 bp upstream from the initiation codon in T6. This inserted fragment was predicted as a lncRNA in *B. napus*. Interestingly, this lncRNA was also found in the ZS11 cultivar reference genome. To evaluate how widespread the lncRNA insertion might be, 421 rapeseed inbred lines were screened with a specific marker, IR (amplified by primers APF and 4R, Supplemental Table S6). Approximately 59.4% of inbred lines had the lncRNA insertion. The transcriptional expression of *BnaA07.HO1* was analyzed in two lines with the lncRNA insert (ZS11 and T6) and two lines without the insert (4942C-5 and Darmor). The transcript level of *BnaA07.HO1* was down-regulated in the lines with the lncRNA insert and up-regulated in the lines without the insert (Fig. 8). It is thus tempting to postulate that the lncRNA insertion in the *BnaA07.HO1* promoter is widespread in *B. napus* and down-regulates the expression of this gene.

To investigate whether the down-regulation of *BnaA07.HO1* contributed to the *ysl* phenotype, the leaf phenotypes of the filial generations from the cross between *ysl* and 4942C-5 were investigated. The BC<sub>1</sub> progenies at the seedling stage displayed an expected Mendelian inheritance ratio of 3:1 (green:yellow plants,  $\chi^2 < \chi^2_{0.05} = 3.84$ ;  $P > 0.05$ ; Supplemental Table S5). The green to yellow phenotype ratio in the F<sub>2</sub> population was approximately 15:1 (Supplemental Table S5), indicating that two loci controlled the *ysl*

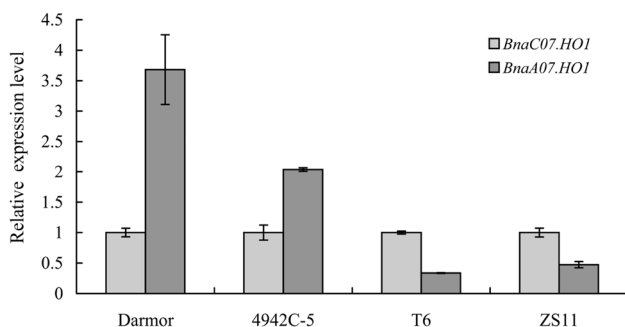


**Fig. 8** Expression levels of *BnaC07.HO1* and *BnaA07.HO1* from inbred lines of Darmor, 4942C-5, T6, and ZS11. Values are showed as the means of three biological replicates and error bars indicate SDs

phenotype through Mendelian inheritance. These results implied that the Chl defect in the *ysl* mutant was caused by not only the loss of *BnaC07.HO1* but also the lncRNA insertion in the *BnaA07.HO1* promoter.

## Discussion

### *BnaC07.HO1* plays an integral role in early development.

Light plays a major signaling role in plant development, and the phys family is one of important photoreceptors for light. Photochemically active phys require the coordination of two spatially separate pathways that synthesize the PHY polypeptides and the PΦB chromophore (Franklin and Quail 2010; Rockwell et al. 2006). The oxidative cleavage of heme by an HO is the committed step in PΦB synthesis in higher plants (Davis et al. 2001). In this study, we successfully identified a heme oxygenase gene, *BnaC07.HO1*, from a chlorophyll-deficient mutant through a map-based cloning approach with the candidate gene strategy. The loss of the *BnaC07.HO1* gene in *ysl* mutant resulted in a reduction of Chl levels in seedlings and produced a yellow-green phenotype. Chl a is required for the formation of the core complexes and light-harvesting complexes (LHCs) in photosystems, whereas Chl b is exclusively included in LHCs in photosystems. And the Chl b biosynthesis is critical for the regulation of the photosynthetic antenna size (Jansson 1994; Tanaka et al. 2001). In the chlorophyll-deficient rice mutant *ysl3*, a complete set of the photosynthesis system components was detected, although the content of PSI and PSII core dimer complexes, LHCII trimer, and light harvesting pigment protein complex was significantly lower than that of the wild type (Tian et al. 2013). In the *Arabidopsis* chlorophyll-deficient mutant *atecb2*, levels of the photosynthetic proteins were significantly reduced or barely detected, whereas transcripts of nuclear-encoded photosynthetic genes were up-regulated (Yu et al. 2009). In *ysl* mutant, the genes associated with photosynthesis were also up-regulated (Fig. 7 and Supplemental Table S4). These indicated that the accumulation of photosynthetic proteins might be affected in the *ysl* and involved in the feedback regulation of photosynthesis gene expression levels.

Previous reports of the yellow-green leaf mutants related to Chl biosynthesis, indicated that a block in Chl biosynthesis resulted in abnormal chloroplasts thylakoid membranes (Sakuraba et al. 2013; Wang et al. 2010; Wu et al. 2007). The mutant *ysl* also had fewer granal stacks and granal membranes in chloroplasts in seedlings (Zhu et al. 2014). Several HO1 mutants (*hyl*, *yg-2*, *pcd1*, *elm2*, and *se5*) exhibited severe photomorphogenic defects at the seedling stage, but these defects became less pronounced at later

developmental stage (Davis et al. 2001; Izawa et al. 2000; Shi et al. 2013; Terry and Kendrick 1996; Weller et al. 1996). In agreement with previous studies, the *ygl* mutant also showed Chl deficiency in seedlings and delayed greening (Zhu et al. 2014). Additionally, *BnaC07.HO1* was highly expressed in seedling leaves (Fig. 3), and the loss of *BnaC07.HO1* affected multiple metabolic pathways (Supplemental Fig. S4). Thus, it is clear that *BnaC07.HO1* plays an integral role in early development of *B. napus*.

### Functional differentiation of *BnaA07.HO1* and *BnaC07.HO1* in *B. napus*

Most orthologous gene pairs in *B. rapa* and *B. oleracea* remain as homeologous pairs in *B. napus* (Chalhoub et al. 2014). As two homologs of *B. napus* HO1, *BnaA07.HO1* and *BnaC07.HO1* are highly similar in their CDS (Fig. 2). The expression pattern analysis showed that *BnaC07.HO1* and *BnaA07.HO1* were highly expressed in seedling leaves (Fig. 3 and Supplemental Fig. S3). Therefore, it was proposed that *BnaC07.HO1* and *BnaA07.HO1* may play similar roles during early development. However, in stem leaves and flowers, *BnaC07.HO1* expression levels were moderate, whereas *BnaA07.HO1* expression levels were extremely low (Fig. 3 and Supplemental Fig. S3). Differences in the expression patterns of *BnaA07.HO1* and *BnaC07.HO1* may be attributed to the discrepancy between their promoter sequences (Supplemental Fig. S2). In (*A*) *thaliana*, more than half of orthologous genes had diverged in expression (Blanc and Wolfe 2004). In (*B*) *napus*, orthologs of *CCD4*, *SMG7* and *ARF18* were also examined for differences in their expression patterns (Li et al. 2015; Liu et al. 2015; Zhang et al. 2015). Divergences in the expression states may have three outcomes: new expression patterns (neofunctionalization), subdivision of expression patterns (subfunctionalization), or loss of expression patterns (pseudogenization) (Li et al. 2005; Moghe and Shiu 2014). We speculated that subfunctionalization might have occurred between *BnaC07.HO1* and *BnaA07.HO1* in *B. napus*.

### The *ygl* phenotype is due to defects in *BnaA07.HO1* and *BnaC07.HO1*

An insertion in the promoter of a gene prevents or reduces the expression of the gene (Fu et al. 2007; Guo and Gan 2006; Mochizuki et al. 2008; Zipfel et al. 2004). In *Arabidopsis*, a promoter insertion line (*cyp38-1*) expressed the *CYP38* transcript at a significantly reduced level, while the *chlM* mutant with a T-DNA insertion in the promoter region down-regulated the *CHLM* mRNA level to 4–7% of the wild-type level (Fu et al. 2007; Mochizuki et al. 2008). Moreover, in the *fls2* mutant, a T-DNA insertion in

the promoter prevented the expression of the *FLS2* gene (Zipfel et al. 2004). In our study, a lncRNA insertion widespread in *B. napus* was present in the T6 *BnaA07.HO1* promoter, reducing its expression (Fig. 7). It is worth noting that *BnaA07.HO1* expression was higher than the *BnaC07.HO1* expression in seedling leaves of the lines without the lncRNA insertion, whereas the opposite trend was observed in the lines with the lncRNA insertion (Fig. 7). The genetic analysis of progeny from a cross of the mutant (with insert) and 4942 C-5 (without insert) provided evidence that the yellow-green phenotype was controlled by two independent recessive genes (Supplemental Table S5). Altogether, these findings suggested that in *B. napus* lines without the insert, the loss of *BnaC07.HO1* and the down-regulation of *BnaA07.HO1* expression produced the *ygl* mutant chlorophyll defect.

### *BnaC07.HO1* regulated Chl biosynthesis by feedback inhibition

In *A. thaliana*, formation of ALA is limited by the activity of glutamyl tRNA reductase (GluTR) (Tanaka et al. 2011). Previous studies in barley have reported that heme directly binds to the N-terminal extension without the catalytic center of GluTR and inhibits its GluTR activity (Pontopidan and Kannangara 1994; Vothknecht et al. 1998). In the *Arabidopsis* mutant *hyl1*, and tomato mutants *au* and *yg-2*, deficiencies in heme degradation caused excessive heme accumulation and suppressed GluTR activity (Goslings et al. 2004; Parks and Quail 1991; Terry and Kendrick 1999). These studies showed that heme is a feedback inhibitor for ALA synthesis (Brzezowski et al. 2015). In this study, our results showed that His-*BnaC07.HO1* acted as a catalyst for the conversion of heme to BV IX $\alpha$ , demonstrating that *BnaC07.HO1* is involved in heme breakdown for the biosynthesis of phytylchromobilin. Based on the RNA-seq analysis of the *ygl* mutant and the positive transgenic TP10 line, expression levels of four genes related to HEMA1 and HEMC (*Arabidopsis* proteins involved in common steps of tetrapyrrole metabolism) were up-regulated in the *ygl* mutant (Figs. 5, 8 and Supplemental Table S2). Additionally, in the Chl biosynthesis branch, eight genes related to CHLI1, CHLI2, CHLM, and PCB2 were also up-regulated in the *ygl* mutant (Figs. 5, 8 and Supplemental Table S2). Therefore, the loss of *BnaC07.HO1* in *ygl* presumably blocked the heme degradation, resulting in excessive heme accumulation, which repressed GluTR activity. The feedback inhibition of ALA formation reduced the tetrapyrrole intermediates in the Chl synthesis branch (Figs. 6, 8, 9). The reduction of Chl a and Chl b levels in the mutant also provided additional support for the hypothesis (Fig. 1). Expression levels of the genes encoding the catalytic enzymes of Chl biosynthesis would be

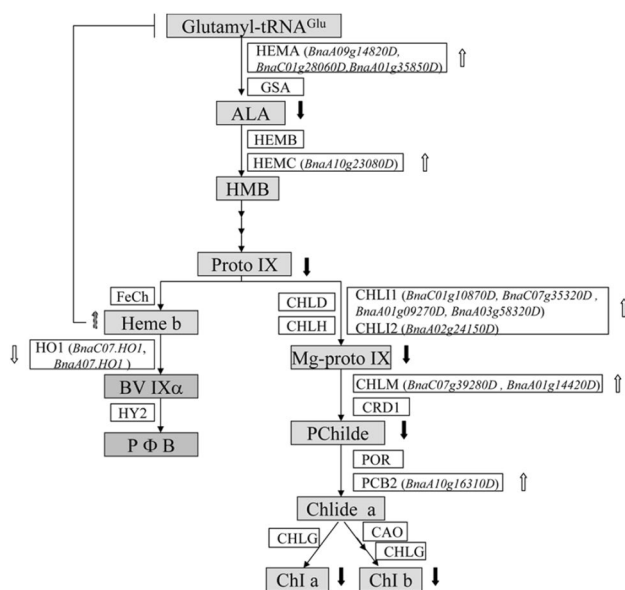


**Fig. 9** The tetrapyrrole pathway with key enzymes and tetrapyrrole intermediates in *ygl* mutant. HEMA, glutamyl-tRNA reductase; ALA, 5-aminolevulinic acid; GSA, glutamate-1-semialdehyde 2,1-aminomutase; HEMB, 5-aminolevulinic acid dehydratase; HEMC, porphobilinogen deaminase; CHLH, Mg-chelatase H subunit; CHLI, Mg-chelatase I subunit; CHLD, Mg-chelatase D subunit; CHLM, Mg-proto IX methyltransferase; CRD1, Mg-proto IX monomethyl-ester cyclase; POR, NADPH:protochlorophyllide oxidoreductase; PCB2, divinyl-protochlorophyllide reductase; CHLG, chlorophyll synthase; CAO, chlorophyllide a oxygenase; FCh, ferrochelatase; HO, heme oxygenase; HY2, phytychromobilin synthase; BV IX $\alpha$ , biliverdin IX $\alpha$ ; PΦB, phytychromobilin

up-regulated to compensate for deficiencies in the intermediates (Fig. 8, 9). These results indicated that *BnaC07.HO1* played a role not only in phytychromobilin biosynthesis but also in Chl biosynthesis in *B.napus*.

**Acknowledgements** We thank Yun Zhang, Yuanlong Wu, and Dongqin Li for technical support, and Qinghua Zhang and Yanjie Xie for helpful suggestions. No conflicts of interest are declared. This research was financially supported by grants from the Modern Agricultural Industrial Technology System (nycytx-00501), the National Science Foundation of China (31501340), the China Postdoctoral Science Foundation (2015M570647), the Natural Science Foundation of Hubei Province Key Program (2014CFA008) and the National Key Research and Development Program of China (2016YFD0101300).

**Author Contributions** L.Z., X.Z., T.F., and J.W. designed the experiments. L.Z., Z.Y., J.G., and J.L. performed the experiments; J.T., J.S., C.M., and B.Y. contributed new reagents or analytic tools; L.Z. and J.W. analyzed the data and wrote the paper.

## References

Andres F, Galbraith DW, Talon M, Domingo C (2009) Analysis of PHOTOPERIOD SENSITIVITY5 sheds light on the role of

phytychromes in photoperiodic flowering in rice. *Plant Physiol* 151:681–690

Arnon DI (1949) Copper enzymes in isolated chloroplasts. polyphenoloxidase in *Beta Vulgaris*. *Plant Physiol* 24:1–15

Audic S, Claverie JM (1997) The significance of digital gene expression profiles. *Genome Res* 7:986–995

Blanc G, Wolfe KH (2004) Functional divergence of duplicated genes formed by polyploidy during *Arabidopsis* evolution. *Plant Cell* 16:1679–1691

Brzezowski P, Richter AS, Grimm B (2015) Regulation and function of tetrapyrrole biosynthesis in plants and algae. *Biochim Biophys Acta* 1847:968–985

Cao ZY, Xuan W, Liu ZY, Li XN, Zhao N, Xu P, Wang Z, Guan RZ, Shen WB (2007) Carbon monoxide promotes lateral root formation in rapeseed. *J Integr Plant Biol* 49:1070–1079

Cao Z, Geng B, Xu S, Xuan W, Nie L, Shen W, Liang Y, Guan R (2011) BnHO1, a haem oxygenase-1 gene from *Brassica napus*, is required for salinity and osmotic stress-induced lateral root formation. *J Exp Bot* 62:4675–4689

Cenkci S, Cigerici IH, Yildiz M, Ozay C, Bozdag A, Terzi H (2010) Lead contamination reduces chlorophyll biosynthesis and genomic template stability in *Brassica rapa* L. *Environ Exp Bot* 67:467–473

Chalhoub B, Denoed F, Liu S, Parkin IA, Tang H, Wang X, Chiquet J, Belcram H, Tong C, Samans B, Correa M, Da Silva C, Just J, Falentin C, Koh CS, Le Clainche I, Bernard M, Bento P, Noel B, Labadie K, Alberti A, Charles M, Arnaud D, Guo H, Daviaud C, Alamery S, Jabbari K, Zhao M, Edger PP, Chelaifa H, Tack D, Lassalle G, Mestiri I, Schnell N, Le Paslier MC, Fan G, Renault V, Bayer PE, Goliz AA, Manoli S, Lee TH, Thi VH, Chalabi S, Hu Q, Fan C, Tollenaere R, Lu Y, Battail C, Shen J, Sidebottom CH, Wang X, Canaguier A, Chauveau A, Berard A, Deniot G, Guan M, Liu Z, Sun F, Lim YP, Lyons E, Town CD, Bancroft I, Wang X, Meng J, Ma J, Pires JC, King GJ, Brunel D, Delourme R, Renard M, Aury JM, Adams KL, Batley J, Snowdon RJ, Tost J, Edwards D, Zhou Y, Hua W, Sharpe AG, Paterson AH, Guan C, Wincker P (2014) Plant genetics. Early allopolyploid evolution in the post-Neolithic *Brassica napus* oilseed genome. *Science* 345:950–953

Chu P, Yan GX, Yang Q, Zhai LN, Zhang C, Zhang FQ, Guan RZ (2015) iTRAQ-based quantitative proteomics analysis of *Brassica napus* leaves reveals pathways associated with chlorophyll deficiency. *J Proteom* 113:244–259

Czarnecki O, Grimm B (2012) Post-translational control of tetrapyrrole biosynthesis in plants, algae, and cyanobacteria. *J Exp Bot* 63:1675–1687

Dal Bosco C, Lezhneva L, Biehl A, Leister D, Strotmann H, Wanner G, Meurer J (2004) Inactivation of the chloroplast ATP synthase gamma subunit results in high non-photochemical fluorescence quenching and altered nuclear gene expression in *Arabidopsis thaliana*. *J Biol Chem* 279:10660–10669

Davis SJ, Bhoo SH, Durski AM, Walker JM, Vierstra RD (2001) The heme-oxygenase family required for phytychrom chromophore biosynthesis is necessary for proper photomorphogenesis in higher plants. *Plant Physiol* 126:656–669

Dixit S, Verma K, Shekhawat GS (2014) In vitro evaluation of mitochondrial-chloroplast subcellular localization of heme oxygenase 1 (HO1) in *Glycine max*. *Protoplasma* 251:671–675

Dun X, Zhou Z, Xia S, Wen J, Yi B, Shen J, Ma C, Tu J, Fu T (2011) BnaC.Tic40, a plastid inner membrane translocon originating from *Brassica oleracea*, is essential for tapetal function and microspore development in *Brassica napus*. *Plant J* 68:532–545

Emborg TJ, Walker JM, Noh B, Vierstra RD (2006) Multiple heme oxygenase family members contribute to the biosynthesis of the phytychrom chromophore in *Arabidopsis*. *Plant Physiol* 140:856–868

- Franklin KA, Quail PH (2010) Phytochrome functions in *Arabidopsis* development. *J Exp Bot* 61:11–24
- Fu A, He ZY, Cho HS, Lima A, Buchanan BB, Luan S (2007) A chloroplast cyclophilin and maintenance of functions in the assembly photosystem II in *Arabidopsis thaliana*. *Proc Natl Acad Sci USA* 104:15947–15952
- Gisk B, Yasui Y, Kohchi T, Frankenberg-Dinkel N (2010) Characterization of the haem oxygenase protein family in *Arabidopsis thaliana* reveals a diversity of functions. *Biochem J* 425:425–434
- Goslings D, Meskauskiene R, Kim C, Lee KP, Nater M, Apel K (2004) Concurrent interactions of heme and FLU with Glu tRNA reductase (HEMA1), the target of metabolic feedback inhibition of tetrapyrrole biosynthesis, in dark- and light-grown *Arabidopsis* plants. *Plant J* 40:957–967
- Guo YF, Gan SS (2006) AtNAP, a NAC family transcription factor, has an important role in leaf senescence. *Plant J* 46:601–612
- Han B, Yang Z, Xie Y, Nie L, Cui J, Shen W (2014) *Arabidopsis* HY1 confers cadmium tolerance by decreasing nitric oxide production and improving iron homeostasis. *Mol Plant* 7:388–403
- Hanke GT, Hase T (2008) Variable photosynthetic roles of two leaf-type ferredoxins in *Arabidopsis*, as revealed by RNA interference. *Photochem Photobiol* 84:1302–1309
- Ito-Maki M, Ishikawa K, Matera KM, Sato M, Ikeda-Saito M, Yoshida T (1995) Demonstration that histidine-25, but not Histidine-132, is the axial heme ligand in rat heme oxygenase-1. *Arch Biochem Biophys* 317:253–258
- Izawa T, Oikawa T, Tokutomi S, Okuno K, Shimamoto K (2000) Phytochromes confer the photoperiodic control of flowering in rice (a short-day plant). *Plant J* 22:391–399
- Jansson S (1994) The light-harvesting chlorophyll a/b-binding proteins. *Biochim Biophys Acta* 1184:1–19
- Jefferson RA, Kavanagh TA, Bevan MW (1987) GUS fusions: beta-glucuronidase as a sensitive and versatile gene fusion marker in higher plants. *EMBO J* 6:3901–3907
- Jin QJ, Yuan XX, Cui WT, Han B, Feng JF, Xu S, Shen WB (2012) Isolation and characterization of a heme oxygenase-1 gene from Chinese cabbage. *Mol Biotechnol* 50:8–17
- Jing B, Heng S, Tong D, Wan Z, Fu T, Tu J, Ma C, Yi B, Wen J, Shen J (2012) A male sterility-associated cytotoxic protein ORF288 in *Brassica juncea* causes aborted pollen development. *J Exp Bot* 63:1285–1295
- Lee HJ, Mochizuki N, Masuda T, Buckhout TJ (2012) Disrupting the bimolecular binding of the haem-binding protein 5 (ATHBP5) to haem oxygenase 1 (HY1) leads to oxidative stress in *Arabidopsis*. *J Exp Bot* 63:5967–5978
- Li WH, Yang J, Gu X (2005) Expression divergence between duplicate genes. *Trends Genet* 21:602–607
- Li S, Chen L, Zhang L, Li X, Liu Y, Wu Z, Dong F, Wan L, Liu K, Hong D, Yang G (2015) BnaC9.SMG7b Functions as a positive regulator of the number of seeds per silique in *Brassica napus* by regulating the formation of functional female gametophytes. *Plant Physiol* 169:2744–2760
- Ling TF, Zhang B, Cui WT, Wu MZ, Lin JS, Zhou WT, Huang JJ, Shen WB (2009) Carbon monoxide mitigates salt-induced inhibition of root growth and suppresses programmed cell death in wheat primary roots by inhibiting superoxide anion overproduction. *Plant Sci* 177:331–340
- Liu J, Hua W, Hu Z, Yang H, Zhang L, Li R, Deng L, Sun X, Wang X, Wang H (2015) Natural variation in ARF18 gene simultaneously affects seed weight and silique length in polyploid rapeseed. *Proc Natl Acad Sci U S A* 112:E5123–E5132
- Lysak MA, Koch MA, Pecinka A, Schubert I (2005) Chromosome triplication found across the tribe Brassiceae. *Genome Res* 15:516–525
- Matsumoto F, Obayashi T, Sasaki-Sekimoto Y, Ohta H, Takamiya K, Masuda T (2004) Gene expression profiling of the tetrapyrrole metabolic pathway in *Arabidopsis* with a mini-array system. *Plant Physiol* 135:2379–2391
- Mochizuki N, Tanaka R, Tanaka A, Masuda T, Nagatani A (2008) The steady-state level of Mg-protoporphyrin IX is not a determinant of plastid-to-nucleus signaling in *Arabidopsis*. *Proc Natl Acad Sci U S A* 105:15184–15189
- Moghe GD, Shiu SH (2014) The causes and molecular consequences of polyploidy in flowering plants. *Ann N Y Acad Sci* 1320:16–34
- Mortazavi A, Williams BA, McCue K, Schaeffer L, Wold B (2008) Mapping and quantifying mammalian transcriptomes by RNA-Seq. *Nat Methods* 5:621–628
- Muramoto T, Kohchi T, Yokota A, Hwang I, Goodman HM (1999) The *Arabidopsis* photomorphogenic mutant hy1 is deficient in phytochrome chromophore biosynthesis as a result of a mutation in a plastid heme oxygenase. *Plant Cell* 11:335–348
- Muramoto T, Tsurui N, Terry MJ, Yokota A, Kohchi T (2002) Expression and biochemical properties of a ferredoxin-dependent heme oxygenase required for phytochrome chromophore synthesis. *Plant Physiol* 130:1958–1966
- Nixon PJ, Michoux F, Yu J, Boehm M, Komenda J (2010) Recent advances in understanding the assembly and repair of photosystem II. *Ann Bot* 106:1–16
- Parkin IA, Lydiat DJ, Trick M (2002) Assessing the level of collinearity between *Arabidopsis thaliana* and *Brassica napus* for A. *thaliana* chromosome 5. *Genome* 45:356–366
- Parkin IA, Gulden SM, Sharpe AG, Lukens L, Trick M, Osborn TC, Lydiat DJ (2005) Segmental structure of the *Brassica napus* genome based on comparative analysis with *Arabidopsis thaliana*. *Genetics* 171:765–781
- Parks BM, Quail PH (1991) Phytochrome-deficient hy1 and hy2 long hypocotyl mutants of *Arabidopsis* are defective in phytochrome chromophore biosynthesis. *Plant Cell* 3:1177–1186
- Peng L, Shikanai T (2011) Supercomplex formation with photosystem I is required for the stabilization of the chloroplast NADH dehydrogenase-like complex in *Arabidopsis*. *Plant Physiol* 155:1629–1639
- Pesaresi P, Scharfenberg M, Weigel M, Granlund I, Schroder WP, Finazzi G, Rappaport F, Masiero S, Furini A, Jahns P, Leister D (2009) Mutants, overexpressors, and interactors of *Arabidopsis* plastocyanin isoforms: revised roles of plastocyanin in photosynthetic electron flow and thylakoid redox state. *Molecular plant* 2:236–248
- Pontoppidan B, Kannangara CG (1994) Purification and partial characterisation of barley glutamyl-tRNA(Glu) reductase, the enzyme that directs glutamate to chlorophyll biosynthesis. *Eur J Biochem* 225:529–537
- Prasad BR, Kumar SV, Nandi A, Chattopadhyay S (2012) Functional interconnections of HY1 with MYC2 and HY5 in *Arabidopsis* seedling development. *BMC Plant Biol* 12:37
- Rockwell NC, Su YS, Lagarias JC (2006) Phytochrome structure and signaling mechanisms. *Annu Rev Plant Biol* 57:837–858
- Sakuraba Y, Rahman ML, Cho SH, Kim YS, Koh HJ, Yoo SC, Paek NC (2013) The rice faded green leaf locus encodes protochlorophyllide oxidoreductase B and is essential for chlorophyll synthesis under high light conditions. *Plant J* 74:122–133
- Santiago-Ong M, Green RM, Tingay S, Brusslan JA, Tobin EM (2001) shy1 is a mutant affected in multiple aspects of photomorphogenesis. *Plant Physiol* 126:587–600
- Sawers RJH, Linley PJ, Gutierrez-Marcos JF, Delli-Bovi T, Farmer PR, Kohchi T, Terry MJ, Brutnell TP (2004) The Elm1 (ZmHy2) gene of maize encodes a phytochromobilin synthase. *Plant Physiol* 136:2771–2781
- Shekhawat GS, Verma K (2010) Haem oxygenase (HO): an overlooked enzyme of plant metabolism and defence. *J Exp Bot* 61:2255–2270

- Shen Q, Jiang M, Li H, Che LL, Yang ZM (2011) Expression of a *Brassica napus* heme oxygenase confers plant tolerance to mercury toxicity. *Plant Cell Environ* 34:752–763
- Shi DY, Zheng X, Li L, Lin WH, Xie WJ, Yang JP, Chen SJ, Jin WW (2013) Chlorophyll deficiency in the maize elongated mesocotyl2 mutant is caused by a defective heme oxygenase and delaying grana stacking. *PLoS ONE* 8(11):e80107
- Sun J, Loehr TM, Wilks A, Ortiz de Montellano PR (1994) Identification of Histidine 25 as the Heme Ligand in Human Liver Heme Oxygenase. *Biochemistry* 33:13734–13740
- Tanaka R, Koshino Y, Sawa S, Ishiguro S, Okada K, Tanaka A (2001) Overexpression of chlorophyllide a oxygenase (CAO) enlarges the antenna size of photosystem II in *Arabidopsis thaliana*. *Plant J* 26:365–373
- Tanaka R, Kobayashi K, Masuda T (2011) Tetrapyrrole Metabolism in *Arabidopsis thaliana*. The *Arabidopsis* book/American Society of Plant Biologists 9:e0145
- Terry MJ (1997) Phytochrome chromophore-deficient mutants. *Plant Cell Environ* 20:740–745
- Terry MJ, Kendrick RE (1996) The aurea and yellow-green-2 mutants of tomato are deficient in phytochrome chromophore synthesis. *J Biol Chem* 271:21681–21686
- Terry MJ, Kendrick RE (1999) Feedback inhibition of chlorophyll synthesis in the phytochrome chromophore-deficient aurea and yellow-green-2 mutants of tomato. *Plant Physiol* 119:143–152
- Tian XQ, Ling YH, Fang LK, Du P, Sang XC, Zhao FM, Li YF, Xie R, He GH (2013) Gene cloning and functional analysis of yellow green leaf3 (*yg13*) gene during the whole-plant growth stage in rice. *Genes Genom* 35:87–93
- Verma K, Dixit S, Shekhawat GS, Alam A (2015) Antioxidant activity of heme oxygenase 1 in *Brassica juncea* (L.) Czern. (Indian mustard) under salt stress. *Turk J Biol* 39:540–549
- Vothknecht UC, Kannangara CG, von Wettstein D (1998) Barley glutamyl tRNA<sub>Glu</sub> reductase: mutations affecting haem inhibition and enzyme activity. *Phytochemistry* 47:513–519
- Wang P, Gao J, Wan C, Zhang F, Xu Z, Huang X, Sun X, Deng X (2010) Divinyl chlorophyll(ide) can be converted to monovinyl chlorophyll(ide) a by a divinyl reductase in rice. *Plant Physiol* 153:994–1003
- Weller JL, Terry MJ, Rameau C, Reid JB, Kendrick RE (1996) The Phytochrome-deficient *pcd1* mutant of pea is unable to convert heme to Biliverdin IX[alpha]. *Plant Cell* 8:55–67
- Weller JL, Terry MJ, Reid JB, Kendrick RE (1997) The phytochrome-deficient *pcd2* mutant of pea is unable to convert biliverdin IX $\alpha$  to 3(Z)-phytychromobilin. *Plant J* 11:1177–1186
- Willemsen V, Wolkenfelt H, de Vrieze G, Weisbeek P, Scheres B (1998) The HOBbit gene is required for formation of the root meristem in the *Arabidopsis embryo*. *Development* 125:521–531
- Wu Z, Zhang X, He B, Diao L, Sheng S, Wang J, Guo X, Su N, Wang L, Jiang L, Wang C, Zhai H, Wan J (2007) A chlorophyll-deficient rice mutant with impaired chlorophyllide esterification in chlorophyll biosynthesis. *Plant Physiol* 145:29–40
- Wu M, Huang J, Xu S, Ling T, Xie Y, Shen W (2011) Haem oxygenase delays programmed cell death in wheat aleurone layers by modulation of hydrogen peroxide metabolism. *J Exp Bot* 62:235–248
- Xie YJ, Xu S, Han B, Wu MZ, Yuan XX, Han Y, Gu Q, Xu DK, Yang Q, Shen WB (2011) Evidence of *Arabidopsis* salt acclimation induced by up-regulation of HY1 and the regulatory role of RbohD-derived reactive oxygen species synthesis. *Plant J* 66:280–292
- Xie YJ, Xu DK, Cui WT, Shen WB (2012) Mutation of *Arabidopsis* HY1 causes UV-C hypersensitivity by impairing carotenoid and flavonoid biosynthesis and the down-regulation of antioxidant defence. *J Exp Bot* 63:3869–3883
- Xie Y, Mao Y, Duan X, Zhou H, Lai D, Zhang Y, Shen WB (2015) *Arabidopsis* HY1-modulated stomatal movement: an integrative hub for its functionally associated with ABI4 in the dehydration-induced ABA responsiveness. *Plant Physiol* 170:1699–1713
- Xu S, Wang L, Zhang B, Han B, Xie Y, Yang J, Zhong W, Chen H, Wang R, Wang N, Cui W, Shen W (2012) RNAi knockdown of rice SE5 gene is sensitive to the herbicide methyl viologen by the down-regulation of antioxidant defense. *Plant Mol Biol* 80:219–235
- Xu L, Hu K, Zhang Z, Guan C, Chen S, Hua W, Li J, Wen J, Yi B, Shen J, Ma C, Tu J, Fu T (2016) Genome-wide association study reveals the genetic architecture of flowering time in rapeseed (*Brassica napus* L.). *DNA Res* 23:43–52
- Xuan W, Zhu FY, Xu S, Huang BK, Ling TF, Qi JY, Ye MB, Shen WB (2008) The heme oxygenase/carbon monoxide system is involved in the auxin-induced cucumber adventitious rooting process. *Plant Physiol* 148:881–893
- Yannarelli GG, Noriega GO, Battle A, Tomaro ML (2006) Heme oxygenase up-regulation in ultraviolet-B irradiated soybean plants involves reactive oxygen species. *Planta* 224:1154–1162
- Yoo SD, Cho YH, Sheen J (2007) *Arabidopsis* mesophyll protoplasts: a versatile cell system for transient gene expression analysis. *Nature protocols* 2:1565–1572
- Yu QB, Jiang Y, Chong K, Yang ZN (2009) AtECB2, a pentatricopeptide repeat protein, is required for chloroplast transcript accD RNA editing and early chloroplast biogenesis in *Arabidopsis thaliana*. *Plant J* 59:1011–1023
- Zhai Q, Li CB, Zheng W, Wu X, Zhao J, Zhou G, Jiang H, Sun J, Lou Y, Li C (2007) Phytochrome chromophore deficiency leads to overproduction of jasmonic acid and elevated expression of jasmonate-responsive genes in *Arabidopsis*. *Plant Cell Physiol* 48:1061–1071
- Zhang B, Liu C, Wang Y, Yao X, Wang F, Wu J, King GJ, Liu K (2015) Disruption of a CAROTENOID CLEAVAGE DIOXYGENASE 4 gene converts flower colour from white to yellow in *Brassica* species. *New Phytol* 206:1513–1526
- Zhao H, Yu L, Huai ZX, Wang XH, Ding GD, Chen SS, Li P, Xu FS (2014) Mapping and candidate gene identification defining BnChd1-1, a locus involved in chlorophyll biosynthesis in *Brassica napus*. *Acta Physiol Plant* 36:859–870
- Zhao L, Jing X, Chen L, Liu YJ, Su YN, Liu TT, Gao CB, Yi B, Wen J, Ma CZ, Tu JX, Zou JT, Fu TD, Shen JX (2015) Tribenuron-methyl induces male sterility through anther-specific inhibition of acetolactate synthase leading to autophagic cell death. *Mol Plant* 8:1710–1724
- Zhao Y, ML W, YZ Z, LF D, T P (2000) A chlorophyll-reduced seedling mutant in oilseed rape, *Brassica napus*, for utilization in F<sub>1</sub> hybrid production. *Plant Breeding* 119:131–135
- Zhu LX, Zeng XH, Chen YL, Yang ZH, Qi LP, Pu YY, Yi B, Wen J, Ma CZ, Shen JX, Tu JX, Fu TD (2014) Genetic characterisation and fine mapping of a chlorophyll-deficient mutant (BnaC.ygl) in *Brassica napus*. *Mol Breeding* 34:603–614
- Zipfel C, Robatzek S, Navarro L, Oakeley EJ, Jones JDG, Felix G, Boller T (2004) Bacterial disease resistance in *Arabidopsis* through flagellin perception. *Nature* 428:764–767